RSC Advances

PAPER

View Article Online
View Journal | View Issue

Cite this: *RSC Adv.*, 2021, **11**, 12568

Achievement of narrow-band blue-emitting phosphors $KScSr_{1-y}Ca_ySi_2O_7:Bi^{3+}$ by the migration of luminescence centers†

Yao Yao, Zhijun Wang,* Lingwei Cao, Mingjie Zheng, Xuejiao Wang, Mengya Zhang, Jia Cui, Zhibin Yang, Wenge Ding* and Panlai Li*

Received 20th February 2021
Accepted 24th March 2021

DOI: 10.1039/d1ra01375k

rsc.li/rsc-advances

In recent years, efforts have been made to develop narrow-band emission phosphors with excellent performance. Herein, a series of $KScSr_{1-y}Ca_ySi_2O_7:0.07Bi^{3+}$ narrow-band phosphors were synthesized by a co-substitution method, and the crystal structure, the occupancy of activated ions and luminescence properties were studied in detail. The substitution of Ca^{2+} for Sr^{2+} ions resulted in the migration of the activated Bi^{3+} from the K site to Sr site, accompanied by the regulation of the emission peak from 410 nm to 455 nm, the peak emission half width from 52 nm to 40 nm, and the color purity from the original 78% to 88%. In addition, a warm white LED with low CCT = 3401 K, CRI = 95.5, and CIE color coordinates of (0.3447, 0.3682) has been obtained through the combination of $KSS_{0.6}C_{0.4}S:0.07Bi^{3+}$ with a commercial green and red phosphor on a UV (370 nm) chip. The results not only provided a strategy based on the manipulation of chemical composition and crystal structure to tune spectral distribution, but also broadens the choice of activators of narrow-band blue-emitting phosphors.

1. Introduction

Phosphor converted white light-emitting diodes (pc-LEDs) are emerging backlight units in modern liquid crystal display (LCD) applications.[1] Over the past decade, many efficient phosphors have been developed, most of these phosphors have wide-band emission. The wavelength of some phosphors exceeds the sensitive area of human eyes (700 nm), resulting in the reduction of the luminous efficiency of pc-LEDs. Therefore, over the years people have been committed to improve the resolution of the LCD, power consumption and color gamut. The luminescence characteristics of light, such as position of emission peak and full-width at half-maximum (FWHM), will directly affect the space of color gamut.[2–6] The improvement of color gamut is a hot issue because it can make the color of LCDs more vivid and attractive to consumers. Phosphors, often with narrow emission bands, can produce a wider gamut. Therefore, in order to obtain a large gamut in the pc-LED backlight, narrow-band emission phosphors with good performance need to be developed.

As early as a few years ago, the special luminescence characteristics of narrow-band phosphors attracted the attention of academic and industrial circles. For example, phosphors like Sr $[Mg_3SiN_4]:Eu^{2+}$ (SMS) and $Sr[Mg_2Al_2N_4]:Eu^{2+}$ (SMA) were reported by Schnick's group, and they presented narrow emission, good luminescence efficient and thermal stability.[7,8] Recently, Hubert's group reported $KLi_3SiO_4:Eu^{2+}$ with a broad-band, near warm white emission (FWHM = 49 nm, λ_{em} = 515 nm) in the same oxide-based system.[9,10] These studies tend to focus on the effects of symmetric cation sites and highly condensed skeletons on the emissive bands, and most of them are doped Eu^{2+} or Mn^{4+} ions. However, these elements, especially Eu^{2+}, are usually reabsorbed in the visible region, resulting in a decrease in luminous efficiency. Therefore, it is necessary to develop a pair of narrow-band blue luminescent phosphors that is highly efficiently absorbed in the NUV region and matched well with NUV commercial LED chips to further improve the performance of LCD.

As a favored sensitizer or an activator in luminescent materials, the spectroscopy of Bi^{3+} ions has been extensively investigated.[11] Compared with rare earth luminescence centers, the absorption of Bi^{3+} is mainly concentrated in the NUV region, with no reabsorption and high energy efficiency. Depending of the nature of the host lattice in which Bi^{3+} ion is inserted, this ion may show either a regular luminescence, a cluster-related luminescence, and so on. The regular Bi^{3+} luminescence results from intra-ionic transitions between the ground $^6s_2$ and first excited $^6s_1{}^6p_1$ configurations. Absorption takes place from $^1S_0$ fundamental state to $^3P_1$, $^3P_2$ and $^1P_1$ excited states.[12,13] Benefiting from its naked 6s and 6p orbits, Bi^{3+} has a broadly adjustable luminescence spectrum, affected by different crystal

National-Local Joint Engineering Laboratory of New Energy Photoelectric Devices, Hebei Key Laboratory of Optic-electronic Information and Materials, College of Physics Science & Technology, Hebei University, Baoding 071002, China. E-mail: wangzj1998@126.com; dwg@hbu.edu.cn; li_panlai@126.com; Tel: +86-312-5977068

† Electronic supplementary information (ESI) available: Table S1 and Fig. S1–S5. See DOI: 10.1039/d1ra01375k

field environments, which opens up great possibilities for ion regulation. For instance, Peng's team reported $CaMoO_4$:Bi^{3+} phosphors, half peak width is about 200 nm, mainly studies the cationic alternative implementation color adjustable launch in 2014.[14] Moreover, they obtained (Y, Sc)(Nb, V)O_4:Bi^{3+} phosphors, which also changed the half-peak width from 120 nm to 230 nm through ion regulation in 2016;[15] In summary, Bi^{3+} ions can not only achieve efficient absorption in the NUV region, but also its naked orbits is very conducive to the matrix composition regulation, so as to obtain phosphors with excellent performance.

In our work, a series of narrow-band blue-emitting phosphors $KScSrSi_2O_7$:xBi^{3+} ($0 < x < 0.13$) and $KScSr_{1-y}Ca_ySi_2O_7$:$0.07Bi^{3+}$ ($0 < y < 0.05$) have been prepared by high temperature solid state reaction. Take advantage of the sensitivity of Bi^{3+} ions to the surrounding coordination environment and crystal field, Ca^{2+} ions were introduced into $KScSrSi_2O$:$0.07Bi^{3+}$ to replace Sr^{2+}, control the occupying selection of activated ion Bi^{3+} from K site to Sr site and the luminescence color was adjusted from purple to blue, the structure rigidity and lattice distortion of $KScSr_{1-y}Ca_ySi_2O_7$:$0.07Bi^{3+}$ were changed by cationic component regulation, and a narrow-band emission with a half-peak width of 40 nm was achieved.

2. Experimental section

2.1 Sample preparation

A series of $KScSrSi_2O_7$:xBi^{3+} (KSSS:xBi^{3+}) ($0 < x < 0.13$) and $KScSr_{1-y}Ca_ySi_2O_7$:$0.07Bi^{3+}$ ($KSS_{1-y}C_y$:$0.07Bi^{3+}$) ($0 < y < 0.5$) phosphors were synthesized by high temperature solid-state method. The raw materials used are K_2CO_3 (99.99%), Sc_2O_3 (99.99%), $SrCO_3$ (99.9%), SiO_2 (99.9%, D50∼10 μm), $CaCO_3$ (99.9%) and Bi_2O_3 (99.99%). The raw materials are weighed and mixed in an agate mortar according to certain stoichiometric and fully ground for 30 minutes. Then the mixed powder samples are transferred into an alumina crucible and sintered at a high temperature of 1200 degrees for 5 h. Finally, all obtained powder samples are naturally cooled to room temperature in the furnace and ground for further experimental measurement.

2.2 Characterization

The phase structure of the sample was characterized by Bruker D8 X-ray diffractometer. The corresponding parameters were as follows: the radiation source was CuKα ($\lambda = 0.15406$ nm), the working voltage and current were 40 kV and 40 mA, respectively. The scanning range was 10–80° and the step was 0.02° per s. And the Findit software and Crystalmaker software were used for the structure. Crystal structure refinements were implemented using General Structure Analysis System (GASA). The emission and excitation spectra of samples were recorded by using a Hitachi F-7000 spectrophotometer equipped with a 450 W xenon lamp as the excitation source. The scanning speed was 1200 nm min^{-1} with a step of 0.2 nm. At room temperature, the decay curves were measured by Horiba FL3 with the width of the incident and outgoing slits is 1 nm, and the width of the slit of the sample is 29 nm.

3. Results and discussion

3.1 Crystal structure characterizations

The XRD patterns of KSSS:xBi^{3+} ($0 < x < 0.13$) and $KSS_{1-y}C_y$:$0.07Bi^{3+}$ ($0 < y < 0.5$) are shown in Fig. S1.† The diffraction peaks of all the samples were consistent with the structure of KSSS standard card, indicating that all the samples were pure phase and the introduction of Bi^{3+} and Ca^{2+} ions did not change the crystal structure of the matrix. According to the rule of ion radius matching, Bi^{3+} ions were expected to occupy the positions of Sr^{2+} and K^+ ions. On account of Bi^{3+} was very sensitive to different coordination environments, the crystal field environment around Bi^{3+} can be changed to achieve the regulation of the luminescence performance of Bi^{3+} doped phosphors. In this paper, the luminescence properties of phosphors were improved by using cationic substitution of Ca^{2+} for Sr^{2+} to adjust the coordination environment around Bi^{3+} ions.

As shown in Fig. 1(a), the crystal structure of $KScSrSi_2O_7$ belongs to the $KMRESi_2O_7$ family (M = Ba^{2+}, Sr^{2+}, RE = Y^{3+}, Sc^{3+}), which belongs to the P_{121}/n_1 space group and consists of a tetrahedron and octahedron containing Si_2O_7 groups and octahedral coordination with Sc atoms ($\langle Sc–O \rangle = 2.12$ Å). The framework of $KMRESi_2O_7$ is based on a ScO_6 octahedron which shares each of its apices with an oxygen atom of the Si_2O_7 group. Adjacent ScO_6 octahedra is connected to each other through Si_2O_7 units, whose Si–Si vectors are oriented parallel to the c axis. This connection creates layers of ScO_6 polyhedra in the x–y plane, furthermore, a three-dimensional framework with 8-coordinated Sr atoms ($\langle Sr–O \rangle = 2.71$ Å) and 9-coordinated K cations ($\langle K–O \rangle = 2.86$ Å) located in voids. The three-dimensional connectivity generates a rigid lattice exhibiting highly condensed network. And the two cations are "stacked" in narrow channels, and they are arranged in strict order.[16] In the $KMRESi_2O_7$ family, KSSS has a relatively small bond angle and bond length, which infers that it has a more rigid structure. There are three cation sites in KSSS, K^+ ($r = 1.55$ Å, CN = 9), Sr^{2+} ($r = 1.26$ Å, CN = 8) and Sc^{3+} ($r = 0.745$ Å, CN = 6). Due to the exposed electron configuration in the outermost layer of Bi^{3+} ion, the luminescence of Bi^{3+} is very sensitive to the surrounding crystal field environment. The different symmetry of multivalent cations (Sr^{2+}/K^+/Sc^{3+}) provide infinite possibilities for controlling the selection of Bi^{3+} at different sites and the regulation of luminescence performance. In order to further prove Bi^{3+} successfully doped into the crystal structure, KSSS:xBi^{3+} were refined with GSAS software, and the refining results were shown in Fig. 1(b). The cross represents the experiment raw data, the red solid line represents the calculated data, the blue solid line represents the difference between the observed data and calculated data, the green solid line represents the Bragg position. This refined result shows that the parameters meet the requirements, in other words, all samples are single phase. Other concentration refining results are shown in the Fig. S2.† It is known that the generation of cationic vacancies should contribute to the shrinkage of the crystal cell volume. The cationic vacancies should be produced when the Sr^{2+} ions positions were occupied by Bi^{3+} ions because of the integral charge balance. It can be expressed by the following formula (1):[17]

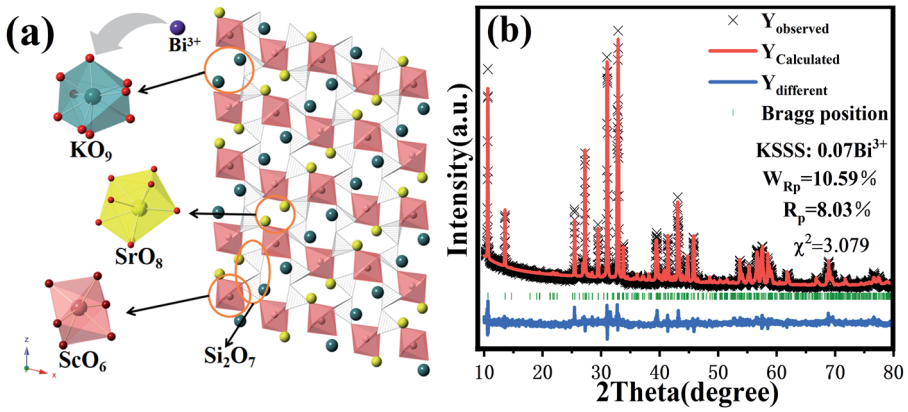

Fig. 1 (a) The crystal structure of $KScSrSi_2O_7$; (b) Rietveld structure refinement patterns of $KScSrSi_2O_7$:0.07Bi^{3+}.

$$Bi^{3+} \rightarrow K^{+} + 2V_{K^{+}}$$
$$2Bi^{3+} \rightarrow 2Sr^{2+} + V_{Sr^{+}} \quad (1)$$

3.2 Luminescence properties of $KScSrSi_2O_7$:xBi^{3+}

Fig. 2(a) shows the emission spectra of KSSS:0.07Bi^{3+} at different excitation wavelengths of 340 nm and 370 nm, as well as the excitation spectra corresponding to the main emission peak of 415 nm and 500 nm. It is obvious that KSSS:0.07Bi^{3+} has a site-selective excitation and its emission spectrum varies with the excitation wavelength. And the excitation spectrum presents a wide 260–400 nm excitation band centering at 280 nm and 370 nm, which indicates that it can be well matched with commercial near ultraviolet LED chips. There are three different cation sites in KSSS crystal, and Bi^{3+} is extremely sensitive to the surrounding coordination environment, therefore, the asymmetric emission may be caused by the substitution of Bi^{3+} for different cation sites. It is generally believed that the doping of Bi ions at trivalent or bivalent sites with coordination number

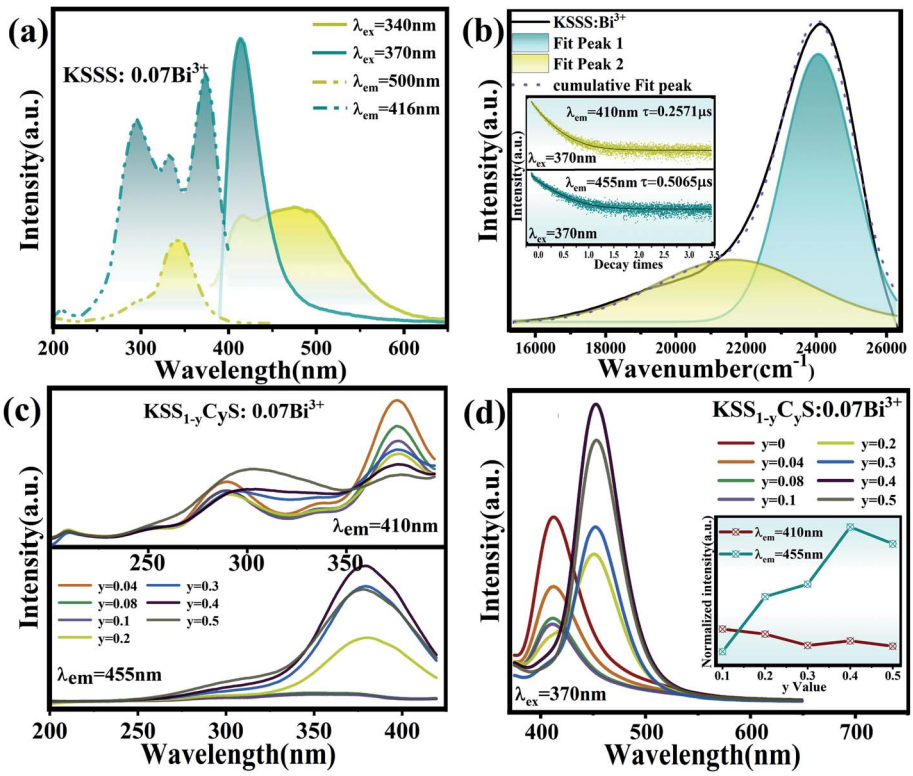

Fig. 2 (a) The different PLE and PL spectra of KSSS:0.07Bi^{3+}. (b) Gaussian fitting of KSSS:0.07Bi^{3+} emission spectra; the inset shows the average life of two sub-emission peaks (410 nm and 455 nm). (c) The PLE spectra of $KSS_{1-y}C_yS$:0.07Bi^{3+} under 410 nm and 455 nm different emission. (d) The PL spectra of $KSS_{1-y}C_yS$:0.07Bi^{3+} under 370 nm excitation; the inset shows the relative excitation intensity *vs.* various Ca^{2+} contents (*y*) at λ_{em} = 410 nm and λ_{em} = 455 nm.

CN larger than or equal to 6 is the most probable.[18] In order to further determine the number of potential luminous centers, the radius percentage difference between the doped ion Bi^{3+} and the potentially substituted ion ($Sr^{2+}/K^{+}/Sc^{3+}$) in KSSS is calculated by using formula (2), and is listed in Table 1.[19]

$$D_r = 100\% \times \left| \frac{R_m(CN) - R_d(CN)}{R_m(CN)} \right| \quad (2)$$

where D_r is the percentage difference of ion radius, CN is the coordination number, R_m (CN) and R_d (CN) are the radii of substituted ions and doped ions, respectively. Since the data of CN = 9 of Bi^{3+} ion is insufficient, a reasonable approximation is provided here. Table 1 presents the R_m (CN), R_d (CN) and D_r values. The corresponding D_r values between Bi^{3+} ions and cations ($K^{+}/Sr^{2+}/Sc^{3+}$) are 20%, 7.1% and 38.2%, respectively, among them, the possibility of Sc^{3+} being replaced is very small and can be ignored. And Bi^{3+} occupies K and Sr sites in $KScSrSi_2O_7$.

According to the number of luminescence centers, the emission band of KSSS:0.07Bi^{3+} can be fitted to two sub-emission peaks, which are located at 410 nm and 455 nm, respectively, as shown in Fig. 2(b). The insets depicts the fluorescence lifetime of the two sub-emission peaks excited by 370 nm pulse laser (nano-LED), which both show second order exponential decay tendency as follows:[21,22]

$$I(t) = A_1 \exp\left(-\frac{t}{\tau_1}\right) + A_2 \exp\left(-\frac{t}{\tau_2}\right) \quad (3)$$

where $I(t)$ is the intensity at t, and τ_1 and τ_2 represent the short and long-decay components while A_1 and A_2 are fitting constants. The average lifetime τ^* can be calculated by the following eqn (4):[20,22]

$$\tau^* = (A_1\tau_1^2 + A_2\tau_2^2)/(A_1\tau_1 + A_2\tau_2) \quad (4)$$

The lifetimes of the two sub-emission peaks (410 nm and 460 nm) are 0.2571 μs and 0.5065 μs, respectively, which are consistent with the lifetimes of Bi^{3+}. The difference in lifetime between different emission peaks confirms the existence of two possible emitting centers. In order to determine the origin of the asymmetric emission peaks, the crystallographic occupancy of ions in the matrix was calculated by using Van Uitert theoretical formula:[23]

$$E = Q\left[1 - \left(\frac{V}{4}\right)^{1/V} 10^{-NRE/80}\right] \quad (5)$$

where E represents the peak (cm^{-1}) of Bi^{3+} ions, Q is the free Bi^{3+} ion at the lower energy edge position, V and E represent the valence and electron affinity of Bi^{3+} ions, respectively. N and R represent the coordination number of the central cation and the radius of the matrix central cation replaced by the activated ion, respectively. Therefore, in the Van Uitert equation, Q, V and E are all inherent attribute parameters of the matrix, hence the size of E only depends on the product of N and R. For K and Sr, the value of $N \times R$ is 13.95 and 10.08, respectively. Since the E value is positively correlated with the $N \times R$, the origin of the two peaks can be qualitatively determined. According to the relation between E value and $N \times R$, the two sub-peaks at 410 nm and 455 nm are generated by Bi^{3+} ions occupying the K and Sr positions, respectively.

For further demonstrate the source of sub-emission peak, the following formula is used to calculate the distance of the centroid shift values of each emission center in KSSS:0.07Bi^{3+} and the crystal field splitting values and total shift values (D(A)) of Bi^{3+} ions at 6s6p level, as follows:[24–27]

$$\varepsilon_C = \frac{e^2}{4\pi\varepsilon_0}\left(\langle r^2\rangle_{6s6p} - \langle r^2\rangle_{6s^2}\right)\sum_{i=2}^{N}\frac{\alpha_{sp}}{\left(R_i - \frac{1}{2}\Delta R\right)^6} \quad (6)$$

$$\alpha_{sp}^{o} = 0.33 + \frac{4.8}{\chi_{av}^{\ 2}} \quad (7)$$

$$\varepsilon_{cfs} = \beta_{poly} R^{-2} \quad (8)$$

$$D(A) = \varepsilon_c(A) + \frac{\varepsilon_{cfs}}{r(A)} - C \quad (9)$$

Formula (6) and (7), $\langle r\rangle$ stands for the radial radius of an electron in 6s6p configuration or $6s^2$ configuration, e is the elementary charge, and ε_0 is the permittivity of vacuum. Thus, the value of $\frac{e^2}{4\pi\varepsilon_0}\left(\langle r^2\rangle_{6s6p} - \langle r^2\rangle_{6s^2}\right)$ is constant. R_i stands for the distance between the center atom and the anion in the lattice. The summation is over all N anions that coordinate Bi^{3+}. $\frac{1}{2}\Delta R$ represents a correction for lattice relaxation around Bi^{3+}, and ΔR for two kinds of cation and activate ion in KSSS radius difference. α_{sp}^{o} is the spectroscopic polarizability of the anion, and its value is 2.82×10^{-30} m^{-3}. χ_{av} is the electronegativity of the cation. In formula (8), β_{poly} is a constant that depends on the type of the coordination polyhedron. In this case, for KSSS:0.07Bi^{3+}, $\beta_{poly} = 1.35 \times 10^9$ pm^2 cm^{-1}. In formula (9), ε_c(A) is the centroid shift, ε_{cfs}(A) is the crystal field splitting. Finally, by formula (9), the total displacement value of energy level in KSSS:0.07Bi^{3+} shows D(K) < D(Sr), the related data are listed in Table 2. Combined with the previous analysis, it is verified again that the sub-emission peaks at 410 nm and 455 nm are derived from the emission of Bi^{3+} ions at K and Sr sites, respectively.

Table 1 Ionic radii difference percentage (D_r) between matrix cations and doped Bi^{3+}

Matrix cation (CN)	R_m (Å)	Doped ion (CN)	R_d (Å)	D_r (%)
K^{+} (9)	1.55	Bi^{3+} (9)	1.24	20
Sr^{2+} (8)	1.26	Bi^{3+} (8)	1.17	7.1
Sc^{3+} (6)	0.745	Bi^{3+} (6)	1.03	38.2

3.3 Controlling site-selection of Bi^{3+} *via* Ca^{2+} substitution for Sr^{2+}

As is known to all, Bi^{3+} ion as a commonly used transition metal doped element, it's 6s and 6p electrons are in the outermost layer of the electron shell, which makes its luminescence properties are easily affected by the surrounding

Table 2 The relative value of the energy level displacement in KSSS:0.07Bi^{3+}

Occupying	K^+	Sr^{2+}
av bond (R)	2.890	2.690
ΔR	0.031	0.009
ε_c(A)	0.477	0.605
ε_{cfs}(A)	2.001	2.309
D(A)	D(K) < D(Sr)	

environment.[28,29] As a consequence, Ca^{2+} ions are introduced to regulate the local lattice and improve the luminescence properties. Fig. 2(c) shows the excitation spectra of $KSS_{1-y}C_y$S:0.07Bi^{3+}. When monitored at 410 nm, the resulting PLE spectrum contained two excitation band peaks at 370 nm (in the 350–420 nm range) and 290 nm (in the 200–350 nm range), and when monitored at 455 nm, the resulting PLE spectrum contains one excitation band peaks at 370 nm (in the range of 300–420 nm), which could be attributed to the electronic transitions from the ground state ($^1S_0$) to the excited state ($^3P_1$) of Bi^{3+} ions. With the concentration of Ca^{2+} (y) increasing, the emission intensities at 410 nm gradually decrease, while the emission intensities of 455 nm gradually increase and reach its maximum value when $y = 0.4$, and finally the concentration quenching occurs, as shown in Fig. 2(d). When Ca^{2+} concentration increased, it is speculated that Bi^{3+} ions may be transferred from one luminescence center to another in $KSS_{1-y}C_y$S crystals. The relationship between the emission intensity (fitting intensity at 410 nm and at 455 nm) and Ca^{2+} concentration is plotted in the inset of Fig. 2(d). The trend of monotonic decrease of emission intensity at 410 nm is in sharp contrast to that at 455 nm, which indicates that the occupation of Bi^{3+} transfers from one crystallization position to another in $KSS_{1-y}C_y$S.

In the above study, the occupying position of Bi^{3+} in the host was confirmed, that is, the 410 nm emission peak comes from the K site occupied by Bi^{3+} ions, and the 455 nm emission peak originates from the Sr site occupied by Bi^{3+} ions. Since the luminescence properties of Bi^{3+} are easily influenced by the surrounding crystal field environment, it is necessary to investigate the structural changes caused by the incorporation of Ca^{2+} ions. The main reason for the structural change is that Ca^{2+} has a smaller ionic radius compared with Sr^{2+}. Firstly, at the Sr^{2+} site, Ca^{2+} with small radius cannot completely coordinate with $8O^{2-}$ ions, leading to Ca^{2+} ions moving towards the surface and the gap of SrO_8 polyhedrons and coordinating with $3O^{2-}$ ions to form an isosceles triangular plane. Secondly, the addition of Ca^{2+} increases the distance between the cations, providing space to accommodate more activated ions. Finally, the introduction of small Ca^{2+} ions not only change the local environment of the lattice but also promote the mobility of the activated ions. Importantly, we used the modification of the SrO_8 polyhedron to stimulate the sensitivity of the activated ion Bi^{3+} to its surrounding crystal field environment, leading to the redistribution of Bi^{3+} at two different cation positions. In order to understand the redistribution of Bi^{3+} ions more accurately, $KSS_{1-y}C_y$S:0.07Bi^{3+} was refined with GASA software. Similarly, $KSS_{1-y}C_y$S:0.07Bi^{3+} were refined with GSAS software, and the refining results were shown in Fig. S3.† All parameters met the experimental requirements. When the small radius of Ca^{2+} (r = 1.12 Å, CN = 8) is used to replace the large radius of Sr^{2+} (r = 1.26 Å, CN = 8) in the crystal, the cell should shrink and the cell parameters decrease. Fig. 3(a) shows the changes of cell volume V and cell parameters a, b and c with Ca^{2+} concentration y increasing, respectively. Curiously, when y increased from 0 to 0.2, both cell parameters and cell volume showed a decreasing trend, but when the replacement concentration was greater than 0.2, each parameter presented an increasing trend. The changes of polyhedron SrO_8 are shown in the illustration. Obviously, the volume of polyhedron SrO_8 also shows a trend of first increase and then decrease, which is due to the gradual entry of Bi^{3+} (r = 1.17 Å, CN = 8) ions with a larger radius into the larger Sr site. In other words, with the gradual substitution of Ca^{2+} for Sr^{2+} ions, Bi^{3+} ions gradually transferred from the K to the Sr site. The schematic diagram of the redistribution of Bi^{3+} in Sr and K sites are presented in Fig. 3(b). When $y < 0.2$, since the radius of Ca^{2+} is smaller than that of Sr^{2+}, and the occupying transfer of Bi^{3+} ion is in the initial stage, the contraction degree of the crystal cell is greater than the expansion degree of the crystal cell, as a result all the parameters of the crystal cell show a state of decrease. When the substitution concentration $y > 0.2$, the expansion caused by the entry of Bi^{3+} ions with large radius into the Sr site is greater than the lattice contraction caused by the replacement of Sr^{2+} ions with Ca^{2+}, hence the crystal cell shows the state of expansion.

According to the above analysis, the emission peaks at 410 nm and 455 nm are originated from Bi^{3+} which occupied the K site and Sr site, respectively. Therefore, the migration of Bi^{3+} ions well explains the change of PL spectrum in Fig. 2(d). As more Bi^{3+} ions transfer from K site to Sr site, the intensity of 455 nm emission increases continuously, while that of 410 nm decreases gradually. When most of Bi^{3+} ions enter the Sr site, the emission intensity will not increase with the increase of Ca^{2+} concentration.

Generally, the luminescence of Bi^{3+} ion has a large absorption cross section and a wide emission due to its s–p transition.[30] Surprisingly, the emission spectra of $KSS_{0.6}C_{0.4}$S:0.07Bi^{3+} shows a narrow-band blue-emission under the excitation of 370 nm, the FWHM is only 40 nm, as shown in Fig. 4(a). Generally, the coordination symmetry and rigidity of the crystal structure are the main factors affect the half-peak width of the emission spectrum, the highly symmetric and rigid structure are more likely to have a narrow emission peak. Conversely, the lower the symmetry of crystal structure, the wider the half-peak width.[31–33] For a polyhedron, the symmetry of the polyhedron is usually characterized by the dispersion degree of the side length. The smaller the dispersion degree of the side length, the higher the symmetry of the polyhedron. The crystal distortion can be expressed by using the set of following equations:[34–36]

$$D(\mathrm{TO}) = \left(\sum_{i=1}^{N}|\mathrm{TO_i} - \mathrm{TO_m}|\right) \Big/ \mathrm{NTO_m}$$
$$D_W = [D(\mathrm{TO_K}) + D(\mathrm{TO_{Sr}})]/2 \quad (10)$$

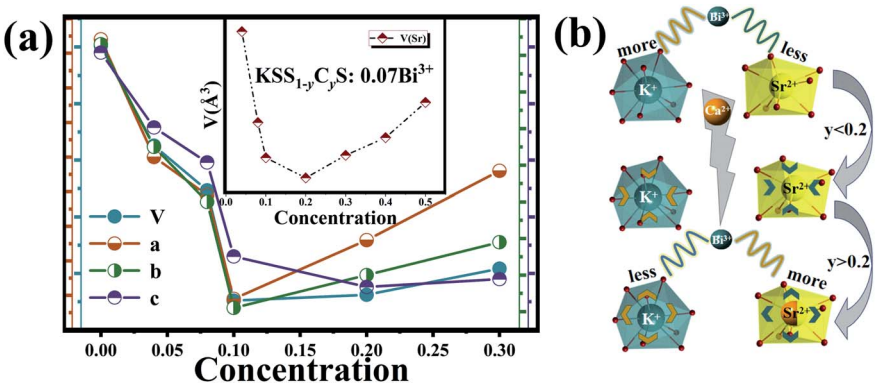

Fig. 3 (a) The changes of cell parameters (*V*, *a*, *b*, *c*) of $KSS_{1-y}C_yS:0.07Bi^{3+}$ with *y* increasing; the inset presents the variation of the volume of the SrO_8 polyhedron. (b) Schematic diagram of the redistribution of Bi^{3+} in Sr and K sites with *y* increasing.

Among them, TO_i is the distances between cations and individual ligand anions, TO_m is the average bond length. The distortion $D(TO)$ is the average deviation of the bond length. D_w is the degree of distortion of the entire crystal, $D(TO_K)$ and $D(TO_{Sr})$ refer to the torsion resistance of polyhedra KO_9 and SrO_8, respectively, and the results are listed in Table 3. Obviously, when Sr^{2+} ions are replaced by Ca^{2+} ions, the distortion degree of SrO_8 polyhedron in $KSS_{1-y}C_yS:0.07Bi^{3+}$ crystal is significantly reduced (As shown in Fig. 4(b)), which indicates that the introduction of Ca^{2+} ions greatly improved the structural rigidity of Sr polyhedron, enhanced the overall symmetry of crystal cells and caused the redistribution of Bi^{3+} ions on the occupied space. With the increase of Ca^{2+} content, the number of Bi^{3+} entering the Sr site increases, while the number of Bi^{3+} at the K site decreases gradually, thus realizing the transfer of the

Table 3 Variation of the distortion degree of $KSS_{1-y}C_yS:0.07Bi^{3+}$ samples

	$y = 0$	$y = 0.04$	$y = 0.08$	$y = 0.10$	$y = 0.20$
D_K	0.112	0.112	0.111	0.112	0.112
D_{Sr}	0.166	0.068	0.068	0.067	0.068
D_W	0.139	0.090	0.090	0.090	0.090

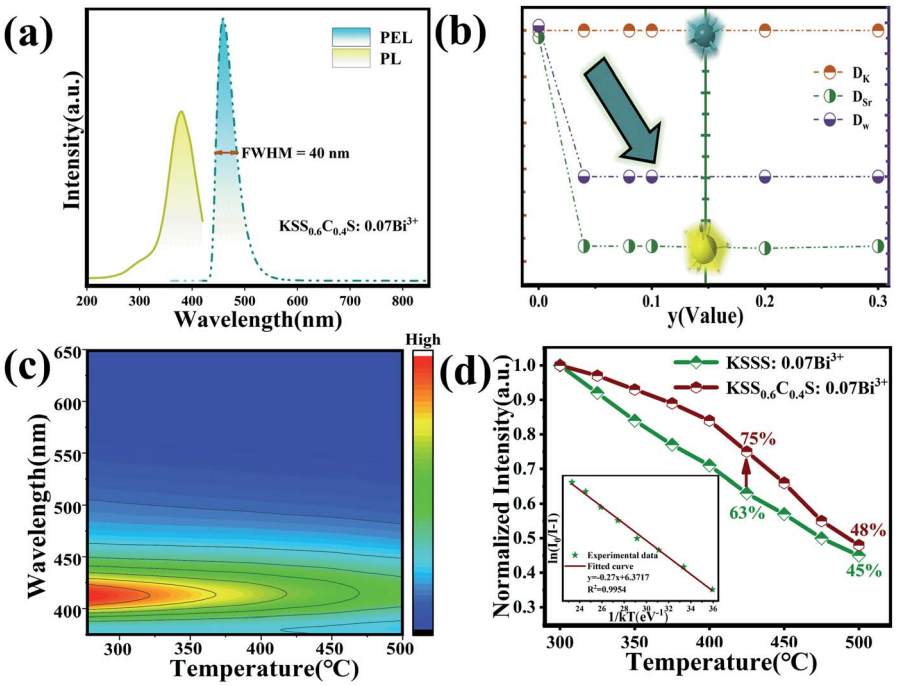

Fig. 4 (a) The emission spectrum of $KSS_{0.6}C_{0.4}S:0.07Bi^{3+}$ ($\lambda_{ex} = 370$ nm). (b) Variation of the distortion degree of $KSS_{1-y}C_yS:0.07Bi^{3+}$ samples. (c) Temperature-dependent emission spectra of $KSS_{0.6}C_{0.4}S:0.07Bi^{3+}$ phosphors under 370 nm excitation. (d) The temperature-dependent normalized integrated emission intensities of $KSSS:0.07Bi^{3+}$ and $KSS_{0.6}C_{0.4}S:0.07Bi^{3+}$; The inset shows the functional relationship of $\ln[(I_0/I_T) - 1]$ *versus* $1/kT$ of $KSS_{0.6}C_{0.4}S:0.07Bi^{3+}$.

main emission peak from 410 nm to 455 nm. The enhancement of structural rigidity and symmetry of the crystal makes the half-peak width of the emission peak significantly narrower.

Debye temperatures for crystallographically distinct atoms ($\theta_{D,i}$) were calculated with isotropic atomic displacement parameters using the high temperature approximation:[37,38]

$$\theta_{D,i} = \sqrt{\frac{3h^2TN_A}{A_i k_B U_{iso,i}}} \quad (11)$$

where i represents the atomic species K or Sr, and A_i is the atomic weight of the atom. The $U_{iso,i}$ values employed were the average of the individual atomic species in the unit cell, weighted by their Wyckoff multiplicities. Then, according to the stoichiometric coefficients of each atom in the formula $KSS_{1-y}C_yS$, the Debye temperature is roughly calculated. It can be seen from the formula that Debye temperature is inversely proportional to atomic displacement parameter (U_{iso}). Relevant parameters can be obtained by using the previous refinement data. The corresponding U_{iso} of K site and Sr site before and after Ca replacement is 0.0397, 0.0419 and 0.0242, 0.0121, respectively. Relevant data are listed in Table S1.† Obviously, when Ca ions replaces Sr^{2+} ions, the average atomic displacement of K site and Sr site decreases, and the reduction of Sr site is particularly significant. The smaller U_{iso} corresponds to the higher Debye temperature. Furthermore, it is proved that when Bi^{3+} ions is transferred from K site to Sr site, the local environment of around Bi^{3+} ions becomes more symmetric and more rigid, which further proves the cause of narrow-band emission after replacement.

Generally, the enhancement of crystal structure rigidity tends to improve the stability of phosphors to a certain extent. To further verify that the introduction of Ca ions increases the structural rigidity of the overall lattice, we measured the temperature spectra of KSSS:0.07Bi^{3+} and $KSS_{0.6}C_{0.4}S$:0.07Bi^{3+}. Fig. 4(c) shows the temperature dependent PL spectra of representative $KSS_{0.6}C_{0.4}S$:0.07Bi^{3+} measured from 300 K to 500 K with a step of 25 K, and the temperature dependent PL spectra of KSSS:0.07Bi^{3+} is shown in Fig. S4.† It is observed that the emission intensity gradually decreases with increasing temperatures due to thermal quenching. The temperature stability of phosphor after Ca^{2+} substitution increased by 12% at a high temperature of 423 K shown in Fig. 4(c). The PL intensity can be fitted by the Arrhenius equation:[39,40]

$$\ln(I_0/I) = \ln A - E_a/kT \quad (12)$$

where, I_0 and I are emission intensities of the sample at 298 K and other test temperatures, respectively. A is a constant, k is Boltzmann's constant, T is the thermodynamic temperature. When taking $1/kT$ as the x-coordinate and $\ln(I_0/I)$ as the y-coordinate, linear fitting was performed on the obtained data. The slope of the fitted line is the activation energy E_a. As is shown in an illustrated of Fig. 4(d), the activation energy E_a of the activated ions in KSSS:0.07Bi^{3+} and $KSS_{0.6}C_{0.4}S$:0.07Bi^{3+} were 0.203 eV and 0.270 eV respectively, which indicated that the phosphors with Ca^{2+} introduction had better thermal stability. It is also further proved that the rigidity of the structure is improved after the introduction of Ca ions, which creates a high rigidity environment for the activated ions.

The luminescence properties of phosphors (*e.g.* peak emission wavelength and full-width at half-maximum (FWHM)) directly affect the color gamut space.[41] As a result, phosphors with narrow half-peak width tend to produce higher color purity, which will be more suitable for high-power pc-LEDs and wide-color backlight applications.[36] The color purity of the phosphor can be defined by the percentage of the chromaticity coordinates of the measured light source and the linear distance between the white light source, which can be calculated by the following formula (13):[42,43]

$$\text{Colour purity} = \sqrt{\frac{(x-x_C)^2+(y-y_C)^2}{(x_D-x_C)^2+(y_D-y_C)^2}} \times 100\% \quad (13)$$

where (x, y) represents the color coordinates of phosphor. C(x_C, y_C) represents the white light source whose CIE color coordinate

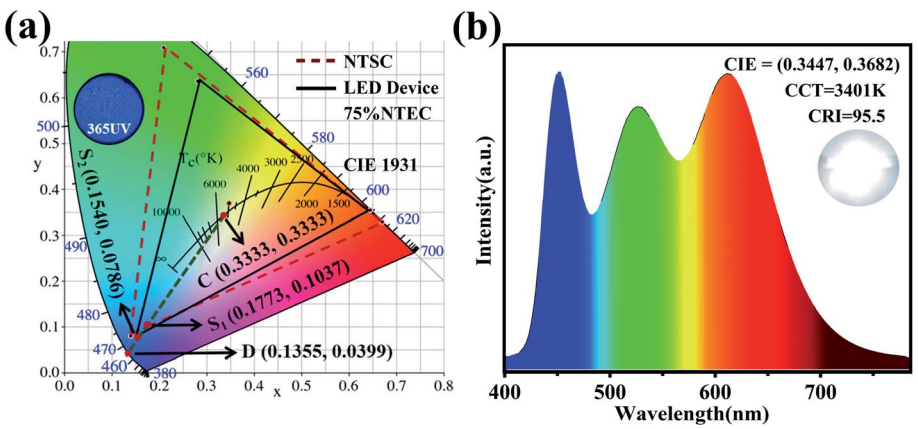

Fig. 5 (a) CIE 1931 color coordinates of main wavelength positions of KSSS:0.07Bi^{3+} and $KSS_{0.6}C_{0.4}S$:0.07Bi^{3+}, color space of NTSC standard (red dotted line) and white LED device (black line), and luminescence photograph of $KSS_{0.6}C_{0.4}S$:0.07Bi^{3+} phosphors under 365 nm UV lamp. (b) The EL spectrum of LED device fabricated with $KSS_{0.6}C_{0.4}S$:0.07Bi^{3+} and the commercial phosphors on an UV LED chip (370 nm) under a voltage of 3.2 V and current of 5 mA.

Table 4 Summary of excitation wavelength, emission wavelength, FWHM, color purity and activation energy (ΔE) of $KSS_{0.6}C_{0.4}S:0.07Bi^{3+}$, some blue narrow-band phosphors and Bi^{3+} doped phosphors previously reported

Samples	λ_{ex} (nm)	λ_{em} (nm)	FWHM (nm)	Color purity (%)	ΔE (eV)	Ref.
$Na_3Sc_2(PO_4)_3:Eu^{2+}$	370	458	50	89	—	44
$Ba_9Lu_{1.5}Al_{0.5}Si_6O_{24}:Ce^{3+}$	400	488	117	—	0.3000	45
$NaHfSi_2O_7:Eu^{2+}$	397	460	54	90	0.1394	46
$RbNa_3(Li_3SiO_4)_4:Eu^{2+}$	400	471	22.4	83.3	—	47
$Ba_5SiO_4Cl_6:Eu^{2+}$	345	440	32	93	0.1425	48
$BaMgAl_{10}O_{17}:Eu^{2+}$	350	450	52	91.3	—	49
$Sr_4OCl_6:Eu^{2+}$	370	446	46	—	0.1378	50
$Ca_5(BO_3)_3F:Bi^{3+}$	322	459	100	—	—	51
$Cs_2AgInCl_6:Bi^{3+}$	380	560	160	—	—	52
$KScSr_{0.6}Ca_{0.4}Si_2O_7:Bi^{3+}$	370	455	40	88	0.2700	—

is (0.3333, 0.3333), as shown in Fig. 5(a), D(x_D, y_D) is the color coordinate of the main wavelength corresponding to the measured light source. It connects the measured light source S_1 ($KSSS:0.07Bi^{3+}$) with white light source C and extends the intersection with the spectral trajectory line at point D. Main wavelength of 465 nm, the comparison wavelength and CIE1931 color coordinates table (x_D, y_D) for (0.1355, 0.0399), S_2 is the color coordinates of $KSSCS:0.07Bi^{3+}$. As a result, the color purity of $KSSS:0.07Bi^{3+}$ and $KSS_{0.6}C_{0.4}S:0.07Bi^{3+}$ are 78% and 88%, respectively. Obviously, the $KSS_{0.6}C_{0.4}S:0.07Bi^{3+}$ phosphors showed better color purity after controlling the cationic component, which indicates that the color purity of the phosphor has been greatly improved by the substitution of Ca^{2+} for Sr^{2+}. Table 4 presents the comparison of luminescent specialties between some phosphors reported previously and $KSS_{0.6}C_{0.4}S:0.07Bi^{3+}$. It is obvious that the color purity of $KSS_{0.6}C_{0.4}S:0.07Bi^{3+}$ is at a medium level. However, comprehensively comparing data such as excitation and emission wavelength, FWHM, color purity and thermal activation energy, it can be found that the performance of $KSS_{0.6}C_{0.4}S:0.07Bi^{3+}$ is at an advantage.

3.4 Applications in white LED backlight display

The wide excitation, narrow emission, and excellent thermal stability make $KSS_{0.6}C_{0.4}S:0.07Bi^{3+}$ a potential candidate for backlight display applications. A white LED was fabricated with $KSS_{0.6}C_{0.4}S:0.07Bi^{3+}$ and the commercial green and red phosphor on an UV (370 nm) chip under a voltage of 3.2 V and current of 5 mA, whose EL spectrum and photograph are shown in Fig. 5(b). It can be seen a warm LED with low CCT = 3401 K, CRI = 95.5, and CIE color coordinate of (0.3447, 0.3682) has been obtained. For a comparison, the EL spectrum and photograph of the commercial blue phosphor $BaMgAl_{10}O_{17}:Eu^{2+}$combined with UV (370 nm) chip are given in Fig. S5.† It is noticeable that the CCT of LED with $KSS_{0.6}C_{0.4}S:0.07Bi^{3+}$ (3401 K) is lower than that of $BaMgAl_{10}O_{17}:Eu^{2+}$ (5064 K), CRI up to 95.5% and CIE color coordinate of (0.4165, 0.4074) had more application potential. The color gamut of tour white LED device can cover the color space of 75% NTSC in CIE 1931 (as shown in Fig. 5(a)), which belongs to the broad gamut category. All these results indicate that $KSSCS:0.07Bi^{3+}$ is a promising narrow-band blue phosphor for display backlight.

4. Conclusions

A series of blue narrow-band phosphors $KScSr_{1-y}Ca_ySi_2O_7:0.07Bi^{3+}$ were obtained by introducing Ca^{2+} ions into $KScSrSi_2O_7:Bi^{3+}$. With Ca^{2+} concentration increasing, the original crystal field environment changed, which lead to the migration of Bi^{3+} from K site to Sr site. Consequently, the main emission peak wavelength changed from 410 nm to 455 nm, and the luminescence color turned from purple to blue. Importantly, the distortion of the polyhedron in the crystal was reduced, the rigidity of the crystal structure was increased, and the symmetry was improved. As a result, under the excitation of 370 nm, $KScSr_{0.6}Ca_{0.4}Si_2O_7:0.07Bi^{3+}$ phosphor presented a blue narrow band emission with a FWHM of 40 nm, and the color purity increased from the original 78% to 88%. And moreover, the LED device using $KScSr_{0.6}Ca_{0.4}Si_2O_7:0.07Bi^{3+}$ phosphor performs a low CCT of 3401 K and a R_a of 95.5. The results demonstrate that the blue narrow-band phosphor $KScSr_{0.6}Ca_{0.4}Si_2O_7:0.07Bi^{3+}$ has a bright prospect for application in pc-LEDs.

Conflicts of interest

The authors declare that they have no conflicts of interest.

Acknowledgements

The work is supported by the National Natural Science Foundation of China (No. 51672066, 51902080), the Funds for Distinguished Young Scientists of Hebei Province, China (No. A2018201101), and the Natural Science Foundation of Hebei Province, China (No. E2019201223), the personnel training project of Hebei Province, China (No. A201902005).

References

1 A. Tücks, A. S. Wochnik, A. K. Henß, C. Scheu, C. Hecht, D. Wiechert, P. J. Schmidt, P. Pust, V. Weiler and

W. Schnick, Narrow-band red-emitting $Sr[LiAl_3N_4]:Eu^{2+}$ as a next-generation LED-phosphor material, *Nat. Mater.*, 2014, **13**, 891–896.

2 P. Pust, P. J. Schmidt and W. Schnick, A revolution in lighting, *Nat. Mater.*, 2015, **14**, 454–458.

3 Z. G. Xia and Q. L. Liu, Progress in discovery and structural design of color conversion phosphors for LEDs, *Prog. Mater. Sci.*, 2016, **84**, 59–117.

4 B. Wang, H. Lin, F. Huang, J. Xu, H. Chen, Z. Lin and Y. Wang, Non-Rare-Earth $BaMgAl_{10-2x}O_{17}:xMn^{4+}$, xMg^{2+}: A Narrow-Band Red Phosphor for Use as a High-Power Warm w-LED, *Chem. Mater.*, 2016, **28**, 3515–3524.

5 J. S. Steckel, J. Ho, C. Hamilton, J. Xi, C. Breen, W. Liu, P. Allen and S. Coe-Sullivan, Ultra-Bright, Highly Efficient, Low Roll-Off Inverted Quantum-Dot Light Emitting Devices (QLEDs), *J. Soc. Inf. Disp.*, 2015, **23**, 294–305.

6 L. Wang, X. Wang, T. Kohsei, K. Yoshimura, M. Izumi, N. Hirosaki and R. J. Xie, High-Uniformity Planar Mini-Chip-Scale Packaged LEDs with Quantum Dot Converter for White Light Source, *Opt. Express*, 2015, **23**, 28707–28717.

7 G. J. Hoerder, M. Seibald, D. Baumann, T. Schroder, S. Peschke, P. C. Schmid, T. Tyborski, P. Pust, I. Stoll, M. Bergler, C. Patzig, S. Reissaus, M. Krause, L. Berthold, T. Hoche, D. Johrendt and H. Huppertz, $Sr[Li_2Al_2O_2N_2]:Eu^{2+}$ A High Performance Red Phosphor to Brighten the Future, *Nat. Commun.*, 2019, **10**, 1824.

8 D. Dutzler, M. Seibald, D. Baumann and H. Huppertz, Alkali Lithosilicates: Renaissance of a Reputable Substance Class with Surprising Luminescence Properties, *Angew. Chem., Int. Ed.*, 2018, **57**, 13676–13680.

9 M. Zhao, H. X. Liao, L. X. Ning, Q. Y. Zhang, Q. L. Liu and Z. G. Xia, Next-Generation Narrow-Band Green-Emitting $RbLi(Li_3SiO_4)_2:Eu^{2+}$ Phosphor for Backlight Display Application, *Adv. Mater.*, 2018, **30**, 1802489.

10 D. Dutzler, M. Seibald, D. Baumann and H. Huppertz, Renaissance of a Reputable Substance Class with Surprising Luminescence Properties, *Angew. Chem., Int. Ed.*, 2018, **57**, 13676.

11 L. L. Wang, Q. Sun, Q. Z. Liu and J. S. Shi, Investigation and application of quantitative relationship between sp energy levels of Bi^{3+} ion and host lattice, *J. Solid State Chem.*, 2012, **191**, 142–146.

12 M. Amer and P. Boutinaud, On the character of the optical transitions in closed-shell transition metal oxides doped with Bi3+, *Phys. Chem. Chem. Phys.*, 2013, **19**(3), 2591–2596.

13 F. W. Kang, G. H. Sun, P. Boutinaud, F. Gao, Z. H. Wang, J. Lu, Y. Y. Li and S. S. Xiao, Tuning the Bi^{3+} photo-emission color over the entire visible region by manipulating secondary cations modulation in the $ScV_xP_{1-x}O_4:Bi^{3+}(0 \leq x \leq 1)$ solid solution, *J. Mater. Chem. C*, 2019, **7**(32), 9865–9877.

14 F. W. Kang, M. Y. Peng, S. H. Xu, Z. J. Ma, G. P. Dong and J. R. Qiu, Broadly Tunable Emission from $CaMoO_4$:Bi Phosphor Based on Locally Modifying the Micro environment Around Bi^{3+} Ions, *Inorg. Chem.*, 2014, 1373–1380.

15 F. W. Kang, H. S. Zhang, W. Lothar, X. B. Yang, Y. Zhang, D. Y. Lei and M. Y. Peng, Band-Gap Modulation in Single Bi^{3+}-Doped Yttrium-Scandium-Niobium Vana dates for Color Tuning over the Whole Visible Spectrum, *Chem. Mater.*, 2016, **28**, 2692–2703.

16 S. Ray, P. Tadge, S. Dutta, T. M. Chen, B. N. Govind and S. J. Dhoble, Luminescence and application of $BaKYSi_2O_7:Eu^{2+}$: A new blue-emitting phosphor for near-UV white-light LED, *Ceram. Int.*, 2018, **44**, 8334–8343.

17 Y. Wang, J. Ding and Y. Wang, Preparation and photo luminescence properties with the site-selected excitation of Bi^{3+} activated $Ba_3Sc_4O_9$ phosphors, *J. Am. Ceram. Soc.*, 2017, **100**, 2612–2620.

18 B. Philippe, On the spectroscopy of Bi^{3+} in d_{10} post-transition metal oxides, *J. Lumin.*, 2020, **223**, 117219.

19 P. Chen, F. Mo, A. Guan, R. Wang, G. Wang, S. Xia and L. Zhou, Luminescence and energy transfer of the color-tunable phosphor $Li_6Gd(BO_3)_3$: Tb^{3+}, Bi^{3+}, Eu^{3+}, *Appl. Radiat. Isot.*, 2016, **108**, 148–153.

20 X. Zhang, J. Xu, Z. Guo and M. Gong, Luminescence and energy transfer of dual-emitting solid solution phosphors $(Ca, Sr)_{10}Li(PO_4)_7:Ce^{3+}$, Mn^{2+} for ratiometric temperature sensing, *Ind. Eng. Chem. Res.*, 2017, **56**, 890–898.

21 M. Li, J. Zhang, J. Han, Z. Qiu, W. Zhou, L. Yu, S. Lian and Z. Li, Changing Ce^{3+} Content and Codoping Mn^{2+} Induced Tunable Emission and Energy Transfer in $Ca_{2.5}Sr_{0.5}$ Al_2O_6: Ce^{3+}, Mn^{2+}, *Inorg. Chem.*, 2017, **56**, 241–251.

22 K. Li, H. Lian, M. Shang and J. Lin, A novel greenish yellow-orange red $Ba_3Y_4O_9:Bi^{3+}$, Eu^{3+} phosphor with efficient energy transfer for UV-LEDs, *Dalton Trans.*, 2015, **44**, 2054–20550.

23 L. G. Van Uitert, An empirical relation fitting the position in energy of the lower d band edge for Eu^{2+} or Ce^{3+} in various compounds, *J. Lumin.*, 1984, **9**, 1.

24 P. Dorenbos, 5d-level energies of Ce^{3+} and the crystalline environment. III. Oxides containing ionic complexes, *Phys. Rev. B: Condens. Matter Mater. Phys.*, 2001, **64**, 125117.

25 F. Wang, W. Wang, L. Zhang, *et al*. Luminescence properties and its red shift of blue-emitting phosphor $Na_3YSi_3O_9:Ce^{3+}$ for UV LED, *RSC Adv.*, 2017, **7**, 27422–27430.

26 P. Dorenbos, Calculation of the energy of the 5d barycenter of $La_3F_3[Si_3O_9]:Ce^{3+}$, *J. Lumin.*, 2003, **105**, 117–119.

27 P. Dorenbos, 5d-level energies of Ce^{3+} and the crystalline environment. I. Fluoride compounds, *Phys. Rev. B: Condens. Matter Mater. Phys.*, 2000, **62**, 15640–15649.

28 F. Kang, M. Peng, S. Xu, Z. Ma, G. Dong and J. Qiu, Broadly tunable emission from $CaMoO_4:Bi^{3+}$ phosphor based on locally modifying the micro environment around Bi^{3+} ions, *Eur. J. Inorg. Chem.*, 2014, 1373–1380.

29 F. Kang, M. Peng, X. Yang, G. Dong, G. Nie, W. Liang, S. Xu and J. Qiu, Broadly tuning Bi^{3+} emission *via* crystal field modulation in solid solution compounds (Y, Lu, Sc) $VO_4:Bi^{3+}$ for ultraviolet converted white LEDs, *J. Mater. Chem. C*, 2014, **2**, 6068–6076.

30 H. Zhu, Z. Xia and H. Liu, Luminescence properties and energy transfer of Bi^{3+}/Eu^{2+}- codoped $Ca_{10}(PO_4)_6F_2$ phosphors, *Mater. Res. Bull.*, 2013, **48**(9), 3513–3517.

31 M. Zhao, Y. Zhou, M. S. Molokeev, Q. Zhang, Q. Liu and Z. G. Xia, Discovery of New Narrow-Band Phosphors with

the UCr_4C_4-Related Type Structure by Alkali Cation Effect, *Adv. Opt. Mater.*, 2019, **7**, 1801631.

32 Q. Wei, X. Zhou and Z. Tang, A novel blue-emitting Eu^{2+}-doped Chlorine silicate phosphor with narrow-band for illumination and displays: structure and luminescence properties, *CrystEngComm*, 2019, **21**, 3660–3667.

33 C. Li, X. Wang and F. Chi, Narrow-Band Blue Emitting Phosphor $Ca_8Mg_7Si_9N_{22}:Eu^{2+}$ for White pc-LEDs, *J. Mater. Chem. C*, 2019, **7**, 3730–3734.

34 J. Ruan, R. J. Xie and N. Hirosaki, Nitrogen gas pressure synthesis and photo luminescent properties of orange-red $SrAlSi_4N_7:Eu^{2+}$ phosphors for white light-emitting diodes, *J. Am. Ceram. Soc.*, 2011, **94**(2), 536–542.

35 Z. G. Xia, S. Mia and M. Chen, Crystallographic Sites, and Tunable Luminescence Properties of Eu^{2+} and Ce^{3+}/Li^{+}-Activated $Ca_{1.65}Sr_{0.35}SiO_4$ Phosphors, *Inorg. Chem.*, 2015, **54**(16), 7684–7691.

36 P. Dai, X. Zhang and L. Bian, Color tuning of $(K_{1-x}Na_x)SrPO_4$: $0.005Eu^{2+}$, yTb^{3+} blue-emitting phosphors *via* crystal field modulation and energy transfer, *J. Mater. Chem. C*, 2013, **1**(2), 4570–4576.

37 N. C. George, A. Birkel and J. Brgoch, Average and Local Structural Origins of the Optical Properties of the Nitride Phosphor $La_{3-x}Ce_xSi_6N_{11}$($0< x \leq 3$), *Inorg. Chem.*, 2013, **52**(23), 1373–13741.

38 N. George, A. Pell and G. Dantelle, Local Environments of Dilute Activator Ions in the Solid-State Lighting Phosphor $Y_{3-x}Ce_xAl_5O_{12}$, *ChemInform*, 2014, **45**(2), 3979–3995.

39 J. Y. Han, I. W. Bin and D. Kim, New full-color-emitting phosphor, Eu^{2+}-doped $Na_{2-x}Al_{2-x}Si_xO_4$ ($0 \leq x \leq 1$) obtained using phase transitions for solid-state white lighting, *J. Mater. Chem.*, 2012, **22**(12), 5374–5381.

40 J. Ruan, R. J. Xie and N. Hirosaki, Nitrogen gas pressure synthesis and photo luminescent properties of orange-red $SrAlSi_4N_7:Eu^{2+}$ phosphors for white light-emitting diodes, *J. Am. Ceram. Soc.*, 2011, **94**(2), 536–542.

41 P. Strobel, S. Schmiechen, M. Siegert, A. Tücks, P. J. Schmidt and W. Schnick, Narrow-Band Green Emitting Nitridolithoalumosilicate $Ba[Li_2(Al_2Si_2)N_6]:Eu^{2+}$ with Framework Topology for LED/LCD Back lighting Applications, *Chem. Mater.*, 2015, **27**, 6109–6115.

42 P. Du and J. S. Yu, Photo luminescence and Cathodoluminescence Properties of Eu^{3+} Ions Activated $AMoO_4$ (A = Mg, Ca, Sr, Ba) Phosphors, *Mater. Res. Bull.*, 2015, **70**, 553–558.

43 Y. F. Wu, Y. T. Nien, Y. J. Wang, I. G. Chen and J. McKittrick, Enhancement of Photo luminescence and Color Purity of $CaTi_3:Eu^{3+}$ Phosphor by Li Doping, *J. Am. Ceram. Soc.*, 2012, **95**, 1360–1366.

44 X. Wang, Z. Zhao, Q. Wu, C. Wang, Q. L. Wang, Y. Yan and Y. Wang, Structure, photo luminescence and abnormal thermal quenching behavior of Eu^{2+}-doped $Na_3Sc_2(PO_4)_3$: a novel blue-emitting phosphor for n-UV LEDs, *J. Mater. Chem. C*, 2016, **4**, 8795–8801.

45 L. Wang, C. Yuan, P. Hu, R. Li, Y. Liu, P. Sun, R. Dong, X. Qi, J. Jiang and H. Jiang, A low cost and high efficient $Ba_9(Lu_{2-x-y}Alx)Si_6O_{24}:yCe^{3+}$ cyan-emitting phosphor, *Ceram. Int.*, 2020, **46**, 11466–11473.

46 Q. Wei, J. Ding and Y. Wang, A novel wide-excitation and narrow-band blue-emitting phosphor with hafnium silicon multiple rings structure for photo luminescence and cathodoluminescence, *J. Alloys Compd.*, 2020, **831**, 154825.

47 H. Liao, M. Zhao, M. S. Molokeev, Q. Liu and Z. G. Xia, Learning from a Mineral Structure toward an Ultra-Narrow-Band Blue-Emitting Silicate Phosphor $RbNa_3(Li_3SiO_4)_4:Eu^{2+}$, *Angew. Chem., Int. Ed. Engl.*, 2018, **57**, 11728–11731.

48 Q. Wei, X. Zhou, Z. Tang, X. Wang and Y. Wang, A novel blue-emitting Eu^{2+}-doped Chlorine silicate phosphor with narrow-band for illumination and displays: structure and luminescence properties, *CrystEngComm*, 2019, **21**, 3660–3667.

49 S. Kim and Y. Kim, Investigation of the degradation mechanisms in $BaMgAl_{10}O_{17}:Eu^{2+}$ phosphor: on the influence of thermal process on operational durability, *Appl. Phys. B*, 2010, **98**, 429–434.

50 S. J. Gwak, P. Arunkumar and W. B. Im, A New Blue-Emitting Oxohalide Phosphor $Sr_4OCl_6:Eu^{2+}$ for Thermally Stable, Efficient White-Light-Emitting Devices under Near-UV, *J. Phys. Chem. C*, 2014, **118**, 2686–2692.

51 X. Li, P. L Li, Z. J. Wang, S. M. Liu, Q. Bao, X. Y. Meng and K. L. Qiu, Color-Tunable Luminescence Properties of Bi^{3+} in $Ca_5(BO_3)_3F$ *via* Changing Site Occupation and Energy Transfer, *Chem. Mater.*, 2017, **29**, 8792–8803.

52 M. B. Gray, J. D. Majher, T. A. Strom and P. M. Woodward, Broadband White Emission in $Cs_2AgIn_{1-x}Bi_xCl_6$ Phosphors, *J. Inorg. Chem.*, 2019, **58**, 13403–13410.